Ionic Mechanisms Underlying the Effects of Vasoactive Intestinal Polypeptide on Canine Atrial Myocardium

Yutao Xi, MD, PhD; Geru Wu, MD, PhD; Tomohiko Ai, MD, PhD; Nancy Cheng, BA; Jurij Matija Kalisnik, MD; Junping Sun, MD; Shahrzad Abbasi, MS; Donghui Yang, MD, PhD; Christopher Fan, BS; Xiaojing Yuan, PhD; Suwei Wang, PhD; MacArthur Elayda, MD, PhD; Igor D. Gregoric, MD, PhD; Bharat K. Kantharia, MD; Shien-Fong Lin, PhD; Jie Cheng, MD, PhD

Background—Vasoactive intestinal polypeptide (VIP) is released from intracardiac neurons during vagal stimulation, ischemia, and heart failure, which are associated with increased vulnerability to atrial fibrillation. VIP shortens atrial effective refractory periods in dogs. Endogenous VIP contributes to vagally mediated acceleration of atrial electric remodeling. VIP is also shown to prolong the duration of acetylcholine-induced atrial fibrillation. However, the ionic mechanisms underlying VIP effects are largely unknown.

Methods and Results—The effects of VIP on transmembrane ion channels were studied in canine atrial cardiomyocytes using patch-clamp techniques. VIP increased delayed rectifier K^+ current and L-type calcium current but decreased the transient outward K^+ current and sodium current. Optical mapping technique was used to assess effects of VIP on action potential durations (APDs) in isolated canine left atria. VIP shortened APD and slowed conduction velocity in a dose-dependent manner. Furthermore, VIP increased spatial heterogeneity of APD and conduction velocity, as assessed by the SDs of APD and conduction velocity, and atrial fibrillation inducibility.

Conclusions—Through its diverse effects on ion channels, VIP shortens APD with increased APD spatial heterogeneity and decreases intra-atrial conduction velocity, which may play an important role in the pathogenesis of atrial arrhythmias in scenarios where VIP release is increased. **(*Circ Arrhythm Electrophysiol*. 2013;6:976-983.)**

Key Words: action potentials ■ atrial fibrillation ■ ion channels ■ vasoactive intestinal polypeptide

Autonomic dysfunction contributes significantly to the pathogenesis of atrial fibrillation (AF).[1,2] Recent studies have demonstrated the importance of ganglionated plexuses and the intrinsic cardiac neural network in the development of AF.[3,4] It has also been demonstrated that neuronally released polypeptides, as integral part of cardiac autonomic innervation, are involved in modulation of cardiac functions.[5] For instance, vasoactive intestinal polypeptide (VIP), a 28-base neural polypeptide found in intracardiac neurons,[6,7] is 50 to 100 times more potent than acetylcholine (ACh) as a vasodilator.[8] Positive inotropic effects of VIP have been ascribed to the activation of L-type calcium channels.[9,10] VIP also accelerates the rate of diastolic depolarization by augmenting pacemaker current (funny current [I_f]).[11] Furthermore, the release of VIP is significantly increased in clinical scenarios with increased incidence of AF such as during vagal stimulation,[12,13] ischemia,[2] and heart failure.[14] VIP shortens atrial and ventricular effective refractory periods in dogs.[15] A recent in vivo study demonstrated that endogenous VIP was accountable for a noncholinergic vagal effect on accelerating the atrial electric remodeling induced by rapid pacing.[13] Recently, VIP was shown to prolong the duration of ACh-induced AF.[16] Our present study was to test the hypothesis that VIP alters the atrial electrophysiological properties through its diverse effects on ion channels and thereby affects vulnerability to AF.

Clinical Perspective on p 983

Methods

The experimental protocol was approved by the Institutional Animal Care and Use Committee in accordance with the Guide for the Care and Use of Laboratory Animals (National Research Council). Recombinant human VIP (Bachem, CA) was used to test the effects of VIP.

Received April 8, 2013; accepted September 10, 2013.

From the Texas Heart Institute/St. Luke's Episcopal Hospital, Houston (Y.X., G.W., N.C., J.M.K., J.S., S.A., D.Y., C.F., S.W., M.E., J.C.); Krannert Institute of Cardiology, Indiana University, Indianapolis (T.A., S.-F.L.); Engineering Technology Department, University of Houston, TX (X.Y.); and Center for Advanced Heart Failure (I.D.G.) and Section of Cardiology (Y.X., B.K.K., J.C.), University of Texas Health Science Center at Houston.

This work was partially presented at the Annual Scientific Sessions of the Heart Rhythm Society in 2009.

The online-only Data Supplement is available at http://circep.ahajournals.org/lookup/suppl/doi:10.1161/CIRCEP.113.000518/-/DC1.

Correspondence to Jie Cheng, MD, PhD, Texas Heart Institute, 6770 Bertner Street, MC 2–255, Houston TX 77030. E-mail jcheng@heart.thi.tmc.edu; or Shien-Fong Lin, PhD, Krannert Institute of Cardiology, Indiana University, 1800 N Capitol Ave, Indianapolis, IN 46202-1239. E-mail linsf@iu.edu

Isolated Canine Atria Preparation

A total of 33 mongrel dogs (weight, 15–20 kg) were used. Hearts were excised quickly after deep anesthesia and full anticoagulation with heparin (30 U/kg). The right coronary and left circumflex artery were cannulated and perfused with a warm (36°C–37°C) oxygenated (95% O_2 and 5% CO_2) Tyrode solution.

Whole-Cell Patch Clamp Technique

The canine atrial myocytes were isolated enzymatically from left atrial tissues, as detailed in the Expanded Methods: Isolation of Canine Atrial Cardiomyocytes in the online-only Data Supplement. Whole-cell voltage-clamp techniques were used to record transmembrane ionic currents at room temperature, including slowly and rapidly activating delayed rectifier K^+ currents (I_{Ks} and I_{Kr}), ultrarapid rectifier K^+ current (I_{Kur}) and transient outward current (I_{to}), sodium current (I_{Na}), and L-type calcium current ($I_{Ca,L}$), as detailed in the Expanded Methods: Whole-Cell Patch Clamp Technique in the online-only Data Supplement.

Optical Mapping

The optical mapping recording system has been described in detail in the Expanded Methods: Optical Mapping in the online-only Data Supplement. The effect of VIP on action potential duration (APD) was assessed from 120×160 sites over a 15×20 mm^2 area in the left atrial free wall. The APDs measured at 20% (APD_{20}), 50% (APD_{50}), 75% (APD_{75}), and 90% (APD_{90}) of its peak repolarization were calculated and compared with and without VIP perfusion. Local conduction velocity (CV) was measured (Expanded Methods: Local Conduction Velocity in the online-only Data Supplement). The SDs of APD_{75} (APD_{75}-SD) and CV (CV-SD) were used as measurements of spatial heterogeneity of APD and CV.

Assessment of Vulnerability to AF in Isolated Canine Atria

Atrial vulnerability to AF was assessed by measuring the inducibility of AF using programmed stimulation (≤3 extra stimuli) after a 20-beat pacing train at a basic drive cycle length of 200 ms (Expanded Methods: Inducibility of AF in the online-only Data Supplement).

Statistics

All data are reported as mean±SEM. Repeated measures ANOVA was used for 3-group comparison (baseline, with VIP, and washout). A general linear mixed effect model was used to evaluate the effects of different VIP concentrations. Categorical data were analyzed using χ^2 test. All statistical analyses were performed using SAS (version 9.3, SAS Inc., Cary, NC). A P value ≤0.05 was considered as statistically significant.

Results

Effects of VIP on Ion Channels in Canine Atrial Cardiomyocytes

Slowly and Rapidly Activating Delayed Rectifier K^+ Currents

Figure 1A illustrated the effect of VIP (1 μmol/L) on I_{Ks} during a representative experiment. Figure 1B illustrates the changes in the current–voltage (I–V) relationship of I_{Ks} in response to VIP. The composite data also demonstrate that VIP (1 μmol/L) significantly increased the peak I_{Ks} current densities at 60 mV (12.78±1.48 pA/pF; n=13) compared with baseline (6.88±0.97 pA/pF; P<0.01) or with washout (6.90±0.95 pA/pF; P<0.01). The tail currents of I_{Ks} (Figure 1C), measured from repolarization to −40 mV, were also significantly increased by VIP (0.68±0.03 pA/pF at VIP 1 μmol/L versus 0.49±0.03 pA/pF at the baseline, P<0.05 and versus 0.53±0.04 pA/pF after washout, P<0.05). However, VIP (1 μmol/L) had no effects on either the peak (P=0.91; n=7) or the tail (P=0.91) of I_{Kr} (Table I in the online-only Data Supplement).

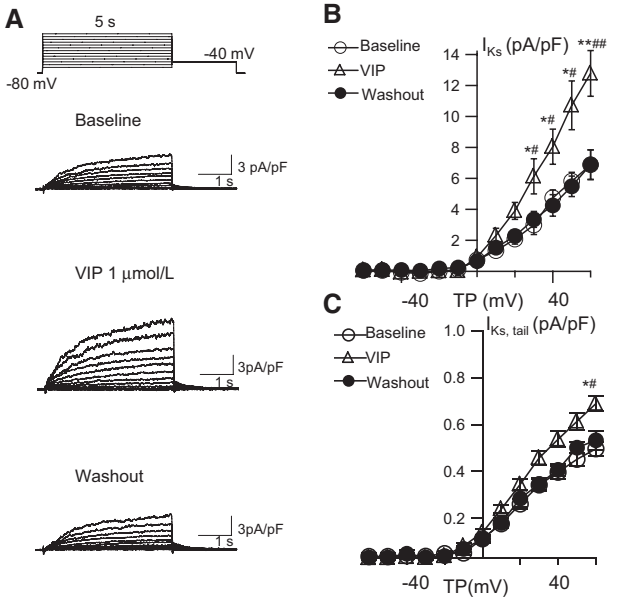

Figure 1. Vasoactive intestinal polypeptide (VIP) increases slowly activating delayed rectifier K^+ current (I_{Ks}). **A**, Representative experiment showing the effect of VIP (1 μmol/L) on I_{Ks}. VIP increased I_{Ks}, which was reversed after washout. **B** and **C**, VIP induced changes in the current–voltage relationships of I_{Ks} and its tail current, respectively, based on the composite data (n=13). VIP increased the tail current of I_{Ks} that was reversed after washout. *P<0.05, **P<0.01 vs baseline; #P<0.05, ##P<0.01 vs washout. TP indicates test pulses.

Ultrarapid Rectifier K^+ Current and Transient Outward Current

As shown in Figure 2, I_{Kur} was elicited with a prepulse at 40 mV for 10 ms that inactivates I_{to} (Figure 2A and 2B).[17] VIP (1 μmol/L) decreased I_{Kur} density (3.29±0.26 pA/pF at 60 mV; n=11) from its values at the baseline (5.95±0.68 pA/pF; P<0.05) and after VIP washout (5.50±0.99 pA/pF; P<0.05; Figure 2D). I_{to} was then determined by digital subtraction of I_{Kur} from total transient activated K^+ current as described previously (Figure 2C).[18] The current densities of I_{to} were significantly decreased by VIP (1 μmol/L; 1.13±0.14 pA/pF at 60 mV; n=11) as compared with its values at the baseline (3.65±0.48 pA/pF; P<0.01) and after VIP washout (2.68±0.43 pA/pF; P<0.01), as shown in Figure 2E and Table I in the online-only Data Supplement.

I_{K1}

I_{K1} (inward rectifier current) was not affected by VIP (1 μmol/L) at any of the tested voltages (P=0.81 versus baseline, and P=0.75 versus washout; n=6).

Sodium Current

VIP (1 μmol/L) significantly decreased the peak of the I_{Na} (−26.92±1.4 pA/pF at −40 mV; n=16) as compared with its values at the baseline (−34.60±1.5 pA/pF; P<0.01) and after VIP washout (−32.14±1.8 pA/pF; P<0.05; Figure 3A and 3B). Furthermore, VIP produced a negative shift in the steady-state

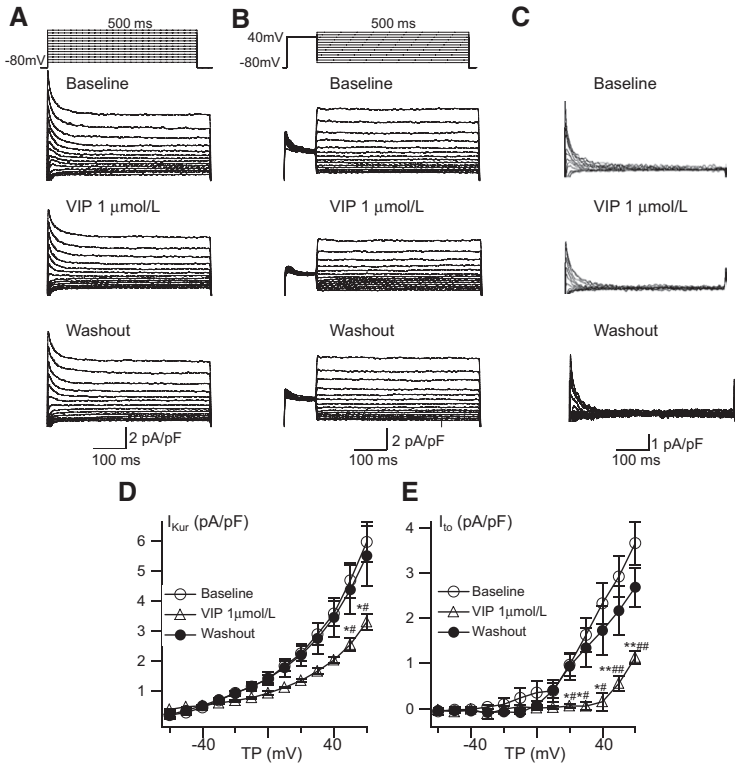

Figure 2. Vasoactive intestinal polypeptide (VIP) decreases transient outward current (I_{to}) and ultrarapid rectifier K^+ current (I_{Kur}). **A**, Whole-cell transient outward K^+ currents were evoked by a 500 ms step-pulse depolarization protocol (between −60 and 60 mV) from a holding potential of −80 mV. **B**, I_{Kur} was obtained with a 40 mV prepulse using a protocol otherwise identical to that used in **A**. **C**, Fast inactivating I_{to} was obtained by subtracting I_{Kur} from transient outward K^+ currents. Changes in the current–voltage relationships of I_{Kur} and I_{to} are depicted in **D** and **E**, respectively, showing that VIP decreased both I_{Kur} and I_{to}. $^*P<0.05$, $^{**}P<0.01$ vs baseline; $^{\#}P<0.05$, $^{\#\#}P<0.01$ vs washout (n=11). TP indicates test pulses.

inactivation curve and a positive shift in the activation curve (Figure 3C, Table II in the online-only Data Supplement).

L-Type Calcium Current

Consistent with the findings from previous study on the ventricular myocytes,[10] VIP (1 μmol/L) significantly increased $I_{Ca,L}$ (−14.11±1.7 pA/pF at 0 mV; n=11) in the canine atrial myocytes as compared with its values at the baseline (−10.54±1.3 pA/pF; $P<0.01$) and after VIP washout (−10.08±1.2 pA/pF; $P<0.01$), but threshold voltage and peak voltage were not affected (Figure 3D and 3E). Steady-state activation and

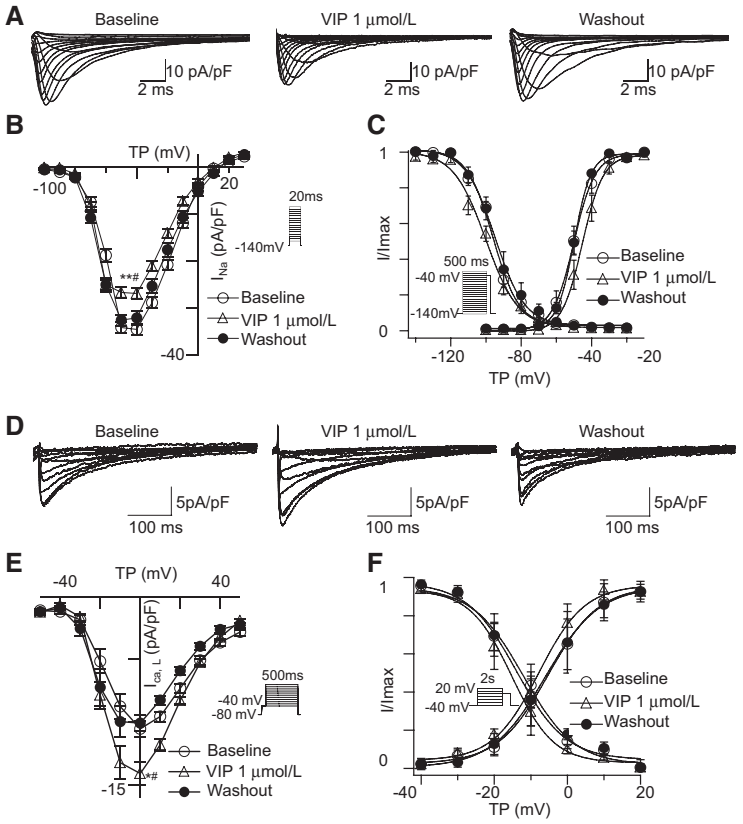

Figure 3. The effects of vasoactive intestinal polypeptide (VIP) on sodium current (I_{Na}) and L-type calcium current ($I_{Ca,L}$). **A**, Representative current traces of I_{Na} in response to VIP. **B**, Changes in the current–voltage response of I_{Na} in response to VIP indicated that I_{Na} was suppressed by VIP (n=16). **C**, Changes in the steady-state inactivation and activation curves of I_{Na} in response to VIP. **D**, Representative current traces of $I_{Ca,L}$ in response to VIP. **E**, Changes in the current–voltage relationship of $I_{Ca,L}$ in response to VIP indicate an increase in $I_{Ca,L}$. **F**, Steady-state inactivation and activation curves of $I_{Ca,L}$. $^*P<0.05$, $^{**}P<0.01$ (peak at −40 mV for I_{Na} and 0 mV for $I_{Ca,L}$) vs baseline; $^{\#}P<0.05$ vs washout (n=11). TP indicates test pulses.

inactivation curves were both shifted more negatively (Figure 3F, Table II in the online-only Data Supplement).

VIP Shortens APD in Canine Atria

In 8 canine atria with intact coronary arterial supply, optical action potentials were recorded from the free wall of the left atrium (Figure 4A) with the VIP perfused in the following sequence: 0.0 μmol/L (baseline), 0.1 μmol/L, 1.0 μmol/L, 10 μmol/L VIP, and then washout, each at 15-minute intervals. Tracings from a representative experiment are shown in Figure 4B: VIP shortened atrial APD in a dose-dependent manner at a drive cycle length of 500 ms. Similarly, the composite data demonstrated that VIP significantly shortened APD_{75} and APD_{90} in a dose-dependent manner for a range of drive cycle lengths ($P<0.001$; Figure 4C, Table III in the online-only Data Supplement).

In a separate group of 4 randomly selected canine atria, stable APDs were recorded every 15 minutes during perfusion with normal Tyrode solution only and showed no significant changes over 1 hour ($P=0.12$; Table IV in the online-only Data Supplement).

VIP Increases APD Spatial Heterogeneity

Figure 5A and 5B shows APD_{75} distribution histograms and maps obtained from a representative experiment. At baseline, the APD_{75} histogram showed a single-mode pattern with a narrow bottom. With VIP at 0.1 and 1.0 μmol/L, APD_{75} distribution assumed a bimodal distribution pattern. At a higher VIP concentration (10 μmol/L), APD_{75} distribution resumed the single-mode pattern that centered on a shorter APD_{75}, likely attributable to receptor saturation.[19] The composite data demonstrated that APD_{75}-SD, as an index of APD heterogeneity, increased significantly during VIP perfusion at different drive cycle lengths (Figure 5C).

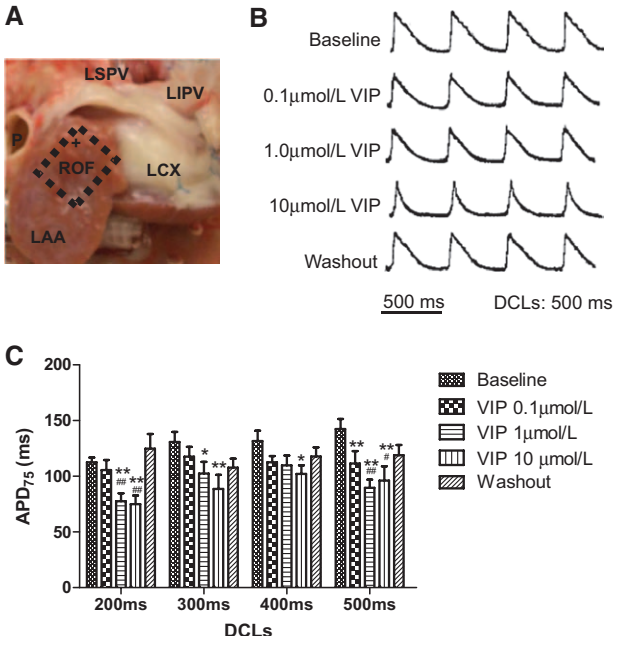

Figure 4. Effects of vasoactive intestinal polypeptide (VIP) on canine atrial action potentials. **A**, A photograph of the left atrial free wall where the optical mapping was recorded. The region of focus (ROF) and the adjacent anatomic markers are shown. Pacing was delivered at the apex of the left atrial appendage. **B**, Representative traces of action potentials recorded from the point marked by "+" courser in **A** after incubation with VIP at 10-fold sequential increases in concentrations showing dose-dependent action potential duration (APD) shortening and partial recovery after 15-minute washout. **C**, The composite data on average APD (APD_{75}) at 4 drive cycle lengths (DCLs) from 8 dogs are shown. Each data point during VIP perfusion was also compared with the baseline and washout where $^{*}P<0.05$, $^{**}P<0.01$ vs baseline; $^{\#}P<0.05$, $^{\#\#}P<0.01$ vs washout. LAA indicates left atrial appendage; LCX, left circumflex artery; and LIPV and LSPV, Left inferior and superior pulmonary vein.

VIP Decreases the Local CV and Increases Its Heterogeneity

The average local CV was calculated at pacing intervals of 200, 300, 400, and 500 ms with different VIP concentrations. VIP significantly decreased local CV in a dose-dependent manner that was partially reversed after 15-minute washout (Figure 6A). Moreover, CV-SD was increased during VIP perfusion (Figure 6B).

VIP Increases Vulnerability to AF in Isolated Canine Atria

Vulnerability to AF was assessed in 11 isolated canine atria. At the baseline, AF was not inducible in any of the atria (0/11). AF was induced in 9 of the same 11 atria during VIP perfusion (1.0 μmol/L; $P<0.01$ versus the baseline) and in only 2 of 8 atria after 15-minute washout ($P=0.16$ versus the baseline; $P<0.05$ versus that during VIP perfusion). AF inducibility could not be assessed after washout in the remaining 3 atria because of sustained AF induced during VIP perfusion that required cardioversion and could in itself affect further AF inducibility. Optical isochrone maps recorded from a representative experiment were shown in Figure 7. With VIP infusion, during extra stimuli at the comparable coupling intervals used at the baseline and after washout, there was evidence for progressive conduction delay/block with VIP perfusion that preceded AF (Figure 7B). Phase map and activation sequence from individual recording sites suggested that this episode of AF was re-entrant around the singularity point (Figure 7D and 7E).

Discussion

The major finding of our study is that VIP shortens APD with increased APD spatial heterogeneity and causes intra-atrial conduction slowing. We have provided the first evidence that these VIP effects can be accounted for by its actions on the repolarizing currents, especially I_{Ks}, and on the sodium current, which may contribute to the increased AF vulnerability.[20,21]

VIP and Atrial Repolarization

Previous in vivo studies indicated that VIP shortened atrial and ventricular effective refractory periods in dogs.[15,22] Although VIP has diverse effects on multiple repolarizing currents (Figures 1 and 2), our study has demonstrated that the overall VIP effect leads to APD abbreviation. VIP-induced increase in I_{Ks} is likely the primary underlying mechanism. In addition, reduced I_{to} in response to VIP could affect early repolarization that may further increase the activation of I_{Ks}.[23]

To the contrary, VIP lengthens atrial APD in rabbit,[24] reflecting a significant species-specific difference in the response

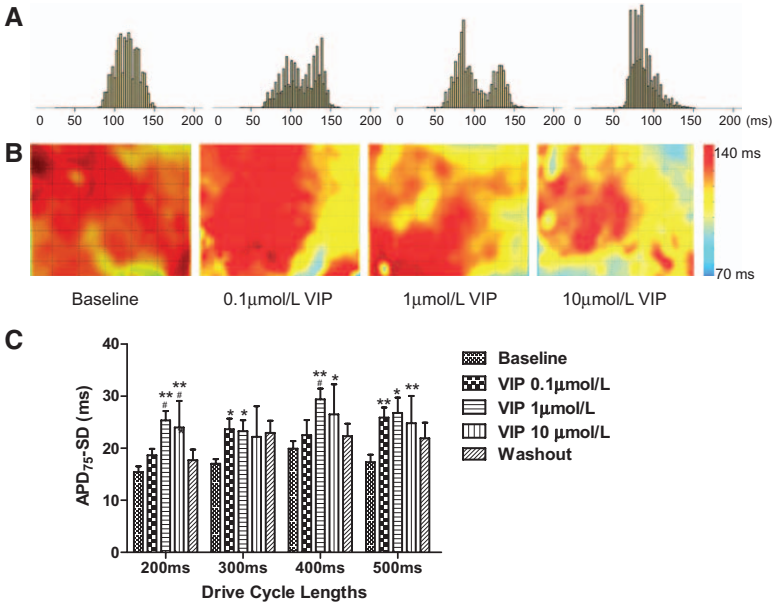

Figure 5. The effects of vasoactive intestinal polypeptide (VIP) on spatial action potential duration (APD) heterogeneity. **A**, A representative histogram shows APD_{75} distribution at drive cycle length of 500 ms. The *x* axis represents the measurement of APD_{75} in milliseconds. **B**, Corresponding action potential duration maps indicate spatial distribution during the same recording as in **A**. **C**, Composite data on the average APD_{75}-SD from 8 dogs at different VIP concentrations and cycle lengths are shown. **P*<0.05, ***P*<0.01 vs baseline; #*P*<0.05 vs washout.

to VIP that necessitated the comparative study with human tissue (Experiments: Results and Figure I in the online-only Data Supplement). VIP shortens APD in both human and canine atrial myocytes. The difference in APD response to VIP between the rabbit atria and the canine/human atria may be related to the complex VIP effects on individual repolarizing currents, especially I_{Ks} and I_{to}, and the differences among species in the relative contributions of these currents to repolarization. VIP increases I_{to} but reduces I_{Ks}. I_{to} is the major outward repolarizing current in rabbit atria where the contribution of I_{Ks} is limited.[25,26] In contrast, in human and canine atria, I_{Ks} contributes more significantly to the repolarization.[27] It was reported that kinetics of I_{Ks} and I_{to} in canine atria are also similar to those in human atrial myocytes.[17]

In addition, VIP increases the spatial APD dispersion as assessed by APD_{75}-SD. Two mechanisms may be involved. First, the contribution of individual K^+ currents, especially I_{Ks} and $I_{to,}$ to atrial repolarization varies among cells within a given region of the heart and also among major anatomic regions.[28] Therefore, the diverse VIP-induced effects on various repolarizing currents may aggravate APD spatial heterogeneity. Second, the uneven distribution of VIP releasing neurons and VIP receptors may also be contributing factors (Experiments: Results and Figure II in the online-only Data Supplement).[10]

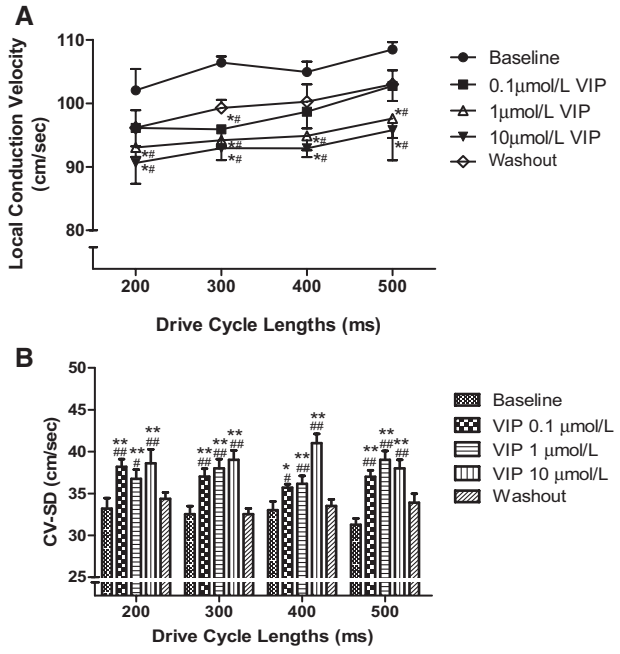

Figure 6. The effects of vasoactive intestinal polypeptide (VIP) on conduction velocity (CV) and its spatial heterogeneity. **A**, Dose-dependent decreases in the CV in response to VIP at different drive cycle lengths and partial recovery after 15-minute washout. **B**, The SD of CV (CV-SD) at each drive cycle length and for each VIP concentration is shown that indicate an increase in CV heterogeneity attributable to VIP. **P*<0.05, ***P*<0.01 vs baseline; #*P*<0.05, ##*P*<0.01 vs washout.

VIP and Intra-Atrial Conduction

Heterogeneous conduction slowing/block predisposes cardiac tissues to re-entrant tachycardia and formation of fibrillatory conduction.[29] Vagally induced conduction delay/block was first described in frogs.[30–32] ACh-induced increase in sink-to-source mismatch has been proposed to account for the vagally induced conduction block.[33] Hirose et al[34] demonstrated that vagal stimulation, during which both ACh and VIP are released concomitantly, could result in intra-atrial conduction delay/block, whereas ACh infusion failed to cause significant conduction delay. Such discrepancy could be explained by the noncholinergic VIP effects during vagal stimulation on conduction. Interestingly, our data also suggested formation of singularity point at the site of VIP-induced conduction block (Figure 7). However, the contribution of VIP effects on I_{Na} to the observed intra-atrial conduction slowing was not quantified in our study. The effect of VIP on the gap junction remains unknown.

Molecular Basis of VIP Effects

VIP exerts its effects through specific VIP receptors: VPAC1 and VPAC2 which are G-protein-coupled receptors and

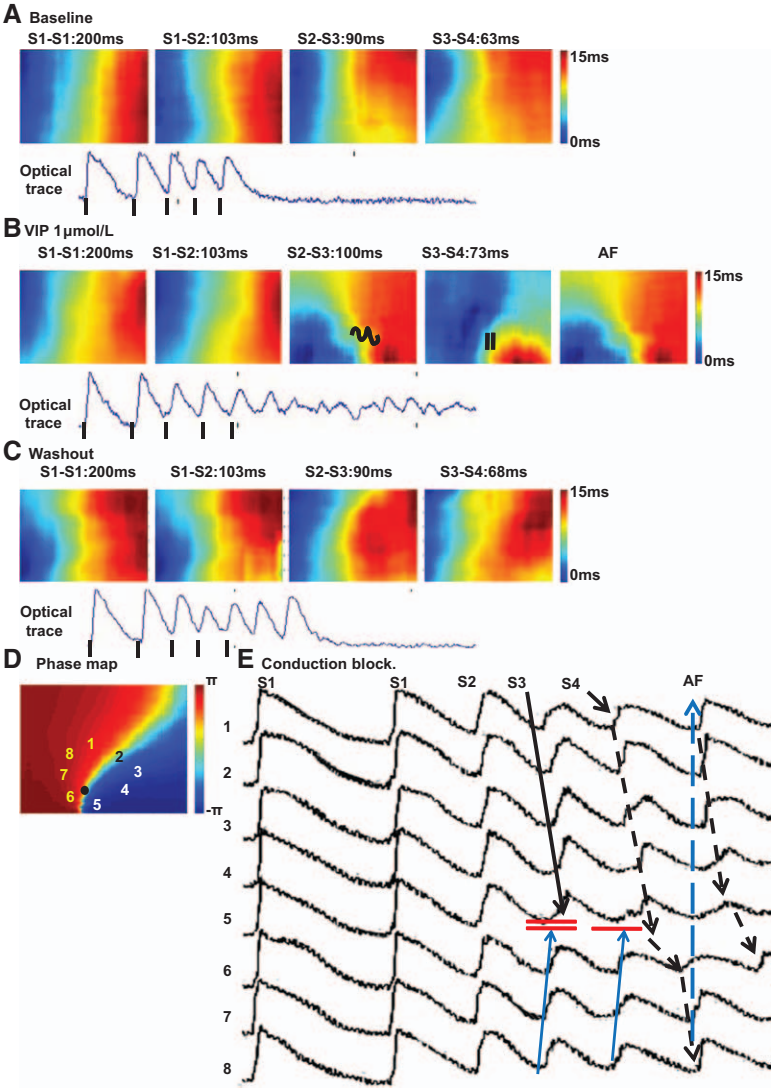

Figure 7. Induced atrial fibrillation (AF). Isochronal map during programmed stimulation (S1–S4) or AF initiation at baseline (**A**), vasoactive intestinal polypeptide (VIP) 1 µmol/L perfusion (**B**), and after 15-minute washout (**C**). The black zigzag and vertical parallel bars in **B** indicate conduction slowing and block. **D**, The phase map generated during the same episode of AF as in **B**, which appears to have been initiated during S3 and S4 and indicates the presence of a singularity point. **E**, The associated tracings taken from **D**, indicates progressive conduction slowing and eventual block with successive extrastimuli that heralded AF.

activate a cAMP/protein kinase A (PKA)-mediated signaling pathway.[35] The observed VIP effects on repolarizing currents are consistent with the known consequences of cAMP/PKA signaling pathway activation.[36,37] However, it was unexpected that VIP suppresses I_{Na} because activation of cAMP/PKA pathway would increase I_{Na}.[38,39] VIP effects through alternative non-PKA signaling pathways, for example, the NO/cyclic GMP and protein tyrosine kinase pathways, have been proposed previously although confirmatory data are lacking.[40,41] Activation of the protein tyrosine kinase pathway was shown to suppress I_{Na} and to reduce conductance through the gap junction.[42,43] Further investigation is warranted to delineate the exact signaling pathway(s) responsible for VIP effects on individual ion channels.

Limitations

The major limitation of our study is that VIP effects were studied in isolation. However, such approach is required to evaluate effects of VIP on individual ionic currents. It is conceivable to speculate that ACh effect on I_{KACh} may dominate over VIP effects on I_{Ks} during vagal stimulation. However, the biological half-life of VIP (in minutes) is longer than that of ACh and the noncholinergic effects of VIP could persist after the direct effects of ACh have dissipated.[13,44,45] Previous studies have also demonstrated significant VIP effects on the heart when endogenous VIP is coreleased with ACh during vagal stimulation.[13,46–48] VIP was also shown to affect ACh-induced AF.[16] Furthermore, the release of endogenous VIP from intracardiac neuron is also increased during ischemia and heart failure where vagal activity is usually not increased.[2,14] Further studies with VIP antagonist during endogenous VIP release are needed to quantify the exact contribution of VIP to the pathogenesis of atrial arrhythmias.

We only performed optical mapping in a small area of the left atrial free wall and did not examine effects of VIP on the myocardium in the right atrium or, more importantly, on the pulmonary vein–left atrial junction which plays an important role in AF. However, the small region of focus in this study was selected to minimize the effects of complicated atrial anatomic structure or anisotropy[49] and to overlap with the region from which myocytes were obtained for VIP receptor expression (Experiments in the online-only Data Supplement). Therefore, the increased heterogeneity of the APD observed in our study is more likely to result from heterogeneity of VIP

receptors among atrial cardiomyocytes or from the diverse VIP effects on repolarizing currents or from both.

Conclusions

Our study provides evidence for novel ionic/cellular mechanisms by which VIP, a neural transmitter released from intracardiac neuron, could alter atrial electrophysiological properties in dogs. We have demonstrated that VIP shortens the atrial APD with increased APD spatial heterogeneity, which may result from heterogeneity of VIP receptor expression and the diverse effects of VIP on ion channels, and impairs intra-atrial conduction. Further studies with endogenous VIP are warranted to delineate the exact contribution of VIP to the pathogenesis of atrial arrhythmias during vagal stimulation, myocardial ischemia, and heart failure.

Acknowledgments

We thank Drs John M. Duncan and David A. Ott from the Texas Heart Institute (THI) for providing human atrial samples.

Sources of Funding

This work was supported by a Grant-in-Aid award from the American Heart Association (11GRNT8000093 to Dr Cheng) and by Indiana University Strategic Research Initiative (Dr Ai).

Disclosures

None.

References

1. Coumel P. Autonomic influences in atrial tachyarrhythmias. *J Cardiovasc Electrophysiol*. 1996;7:999–1007.
2. Jons C, Raatikainen P, Gang UJ, Huikuri HV, Joergensen RM, Johannesen A, Dixen U, Messier M, McNitt S, Thomsen PE; Cardiac Arrhythmias and Risk Stratification after Acute Myocardial Infarction (CARISMA) Study Group. Autonomic dysfunction and new-onset atrial fibrillation in patients with left ventricular systolic dysfunction after acute myocardial infarction: a CARISMA substudy. *J Cardiovasc Electrophysiol*. 2010;21:983–990.
3. Scherlag BJ, Yamanashi W, Patel U, Lazzara R, Jackman WM. Autonomically induced conversion of pulmonary vein focal firing into atrial fibrillation. *J Am Coll Cardiol*. 2005;45:1878–1886.
4. Choi EK, Shen MJ, Han S, Kim D, Hwang S, Sayfo S, Piccirillo G, Frick K, Fishbein MC, Hwang C, Lin SF, Chen PS. Intrinsic cardiac nerve activity and paroxysmal atrial tachyarrhythmia in ambulatory dogs. *Circulation*. 2010;121:2615–2623.
5. Anderson FL, Hanson GR, Reid B, Thorpe M, Kralios AC. VIP and NPY in canine hearts. Distribution and effect of total and selective parasympathetic denervation. *Am J Physiol*. 1993;265(1 pt 2):H91–H95.
6. Kuncová J, Slavíková J, Reischig J. Distribution of vasoactive intestinal polypeptide in the rat heart: effect of guanethidine and capsaicin. *Ann Anat*. 2003;185:153–161.
7. Gordon L, Wharton J, Gaer JA, Inglis GC, Taylor KM, Polak JM. Quantitative immunohistochemical assessment of bovine myocardial innervation before and after cryosurgical cardiac denervation. *Cardiovasc Res*. 1993;27:318–326.
8. Brum JM, Bove AA, Sufan Q, Reilly W, Go VL. Action and localization of vasoactive intestinal peptide in the coronary circulation: evidence for nonadrenergic, noncholinergic coronary regulation. *J Am Coll Cardiol*. 1986;7:406–413.
9. Rigel DF, Grupp IL, Balasubramaniam A, Grupp G. Contractile effects of cardiac neuropeptides in isolated canine atrial and ventricular muscles. *Am J Physiol*. 1989;257(4 Pt 2):H1082–H1087.
10. Tiaho F, Nerbonne JM. VIP and secretin augment cardiac L-type calcium channel currents in isolated adult rat ventricular myocytes. *Pflugers Arch*. 1996;432:821–830.
11. Chang F, Yu H, Cohen IS. Actions of vasoactive intestinal peptide and neuropeptide Y on the pacemaker current in canine Purkinje fibers. *Circ Res*. 1994;74:157–162.
12. Hogan K, Markos F. Vasoactive intestinal polypeptide receptor antagonism enhances the vagally induced increase in cardiac interval of the rat atrium *in vitro*. *Exp Physiol*. 2006;91:641–646.
13. Yang D, Xi Y, Ai T, Wu G, Sun J, Razavi M, Delapasse S, Shurail M, Gao L, Mathuria N, Elayda M, Cheng J. Vagal stimulation promotes atrial electrical remodeling induced by rapid atrial pacing in dogs: evidence of a noncholinergic effect. *Pacing Clin Electrophysiol*. 2011;34:1092–1099.
14. Hershberger RE, Anderson FL, Bristow MR. Vasoactive intestinal peptide receptor in failing human ventricular myocardium exhibits increased affinity and decreased density. *Circ Res*. 1989;65:283–294.
15. Rigel DF, Lathrop DA. Vasoactive intestinal polypeptide facilitates atrioventricular nodal conduction and shortens atrial and ventricular refractory periods in conscious and anesthetized dogs. *Circ Res*. 1990;67:1323–1333.
16. Liu Y, Scherlag BJ, Fan Y, Varma V, Male S, Chaudhry MA, Huang C, Po SS. Inducibility of atrial fibrillation after GP ablations and "autonomic blockade": evidence for the pathophysiological role of the nonadrenergic and noncholinergic neurotransmitters. *J Cardiovasc Electrophysiol*. 2013;24:188–195.
17. Yue L, Feng J, Li GR, Nattel S. Transient outward and delayed rectifier currents in canine atrium: properties and role of isolation methods. *Am J Physiol*. 1996;270(6 pt 2):H2157–H2168.
18. Brouillette J, Clark RB, Giles WR, Fiset C. Functional properties of K+ currents in adult mouse ventricular myocytes. *J Physiol*. 2004;559(pt 3):777–798.
19. Mao YK, Tougas G, Barnett W, Daniel EE. VIP receptors on canine submucosal synaptosomes. *Peptides*. 1993;14:1149–1152.
20. Daoud EG, Bogun F, Goyal R, Harvey M, Man KC, Strickberger SA, Morady F. Effect of atrial fibrillation on atrial refractoriness in humans. *Circulation*. 1996;94:1600–1606.
21. Wijffels MC, Kirchhof CJ, Dorland R, Allessie MA. Atrial fibrillation begets atrial fibrillation. A study in awake chronically instrumented goats. *Circulation*. 1995;92:1954–1968.
22. Pickoff AS, Wang SN, Stolfi A, Ramage D, Ross-Ascuitto NT, Kydon DW, Ascuitto RJ. Vasoactive intestinal peptide: electrophysiologic activity in the newborn heart. *Pediatr Res*. 1994;35:244–249.
23. Grant AO. Cardiac ion channels. *Circ Arrhythm Electrophysiol*. 2009;2:185–194.
24. Halimi F, Piot O, Guize L, Le Heuzey JY. Electrophysiological effects of vasoactive intestinal peptide in rabbit atrium: a modulation of acetylcholine activity. *J Mol Cell Cardiol*. 1997;29:37–44.
25. Giles WR, Imaizumi Y. Comparison of potassium currents in rabbit atrial and ventricular cells. *J Physiol*. 1988;405:123–145.
26. Muraki K, Imaizumi Y, Watanabe M, Habuchi Y, Giles WR. Delayed rectifier K+ current in rabbit atrial myocytes. *Am J Physiol*. 1995;269(2 pt 2):H524–H532.
27. Wang Z, Fermini B, Nattel S. Delayed rectifier outward current and repolarization in human atrial myocytes. *Circ Res*. 1993;73:276–285.
28. Brahmajothi MV, Morales MJ, Liu S, Rasmusson RL, Campbell DL, Strauss HC. In situ hybridization reveals extensive diversity of K+ channel mRNA in isolated ferret cardiac myocytes. *Circ Res*. 1996;78:1083–1089.
29. Akar FG, Spragg DD, Tunin RS, Kass DA, Tomaselli GF. Mechanisms underlying conduction slowing and arrhythmogenesis in nonischemic dilated cardiomyopathy. *Circ Res*. 2004;95:717–725.
30. Rosenshtraukh LV, Zaitsev AV, Fast VG, Pertsov AM, Krinsky VI. Vagally induced block and delayed conduction as a mechanism for circus movement tachycardia in frog atria. *Circ Res*. 1989;64:213–226.
31. Michael G, Xiao L, Qi XY, Dobrev D, Nattel S. Remodelling of cardiac repolarization: how homeostatic responses can lead to arrhythmogenesis. *Cardiovasc Res*. 2009;81:491–499.
32. Burstein B, Comtois P, Michael G, Nishida K, Villeneuve L, Yeh YH, Nattel S. Changes in connexin expression and the atrial fibrillation substrate in congestive heart failure. *Circ Res*. 2009;105:1213–1222.
33. Mansour M, Mandapati R, Berenfeld O, Chen J, Samie FH, Jalife J. Left-to-right gradient of atrial frequencies during acute atrial fibrillation in the isolated sheep heart. *Circulation*. 2001;103:2631–2636.
34. Hirose M, Carlson MD, Laurita KR. Cellular mechanisms of vagally mediated atrial tachyarrhythmia in isolated arterially perfused canine right atria. *J Cardiovasc Electrophysiol*. 2002;13:918–926.
35. Dickson L, Finlayson K. VPAC and PAC receptors: From ligands to function. *Pharmacol Ther*. 2009;121:294–316.
36. Heijman J, Spätjens RL, Seyen SR, Lentink V, Kuijpers HJ, Boulet IR, de Windt LJ, David M, Volders PG. Dominant-negative control of cAMP-dependent IKs upregulation in human long-QT syndrome type 1. *Circ Res*. 2012;110:211–219.

37. Zhang L, Xu CQ, Hong Y, Zhang JL, Liu Y, Zhao M, Cao YX, Lu YJ, Yang BF, Shan HL. Propranolol regulates cardiac transient outward potassium channel in rat myocardium via cAMP/PKA after short-term but not after long-term ischemia. *Naunyn Schmiedebergs Arch Pharmacol*. 2010;382:63–71.
38. Ono K, Kiyosue T, Arita M. Isoproterenol, DBcAMP, and forskolin inhibit cardiac sodium current. *Am J Physiol*. 1989;256(6 pt 1):C1131–C1137.
39. Frohnwieser B, Chen LQ, Schreibmayer W, Kallen RG. Modulation of the human cardiac sodium channel alpha-subunit by cAMP-dependent protein kinase and the responsible sequence domain. *J Physiol*. 1997;498 (pt 2):309–318.
40. Bokaei PB, Ma XZ, Byczynski B, Keller J, Sakac D, Fahim S, Branch DR. Identification and characterization of five-transmembrane isoforms of human vasoactive intestinal peptide and pituitary adenylate cyclase-activating polypeptide receptors. *Genomics*. 2006;88:791–800.
41. Henning RJ, Sawmiller DR. Vasoactive intestinal peptide: cardiovascular effects. *Cardiovasc Res*. 2001;49:27–37.
42. Ahern CA, Zhang JF, Wookalis MJ, Horn R. Modulation of the cardiac sodium channel NaV1.5 by Fyn, a Src family tyrosine kinase. *Circ Res*. 2005;96:991–998.
43. Shen Y, Khusial PR, Li X, Ichikawa H, Moreno AP, Goldberg GS. SRC utilizes Cas to block gap junctional communication mediated by connexin43. *J Biol Chem*. 2007;282:18914–18921.
44. Bösche LI, Wellner-Kienitz MC, Bender K, Pott L. G protein-independent inhibition of GIRK current by adenosine in rat atrial myocytes overexpressing A1 receptors after adenovirus-mediated gene transfer. *J Physiol*. 2003;550(pt 3):707–717.
45. Domschke S, Domschke W, Bloom SR, Mitznegg P, Mitchell SJ, Lux G, Strunz U. Vasoactive intestinal peptide in man: pharmacokinetics, metabolic and circulatory effects. *Gut*. 1978;19:1049–1053.
46. Hill MR, Wallick DW, Martin PJ, Levy MN. Effects of repetitive vagal stimulation on heart rate and on cardiac vasoactive intestinal polypeptide efflux. *Am J Physiol*. 1995;268(5 pt 2):H1939–H1946.
47. Henning RJ, Feliciano L, Coers CM. Vagal nerve stimulation increases right ventricular contraction and relaxation and heart rate. *Cardiovasc Res*. 1996;32:846–853.
48. Saetrum Opgaard O, Knutsson M, de Vries R, Tom B, Saxena PR, Edvinsson L. Vasoactive intestinal peptide has a direct positive inotropic effect on isolated human myocardial trabeculae. *Clin Sci (Lond)*. 2001;101:637–643.
49. Koura T, Hara M, Takeuchi S, Ota K, Okada Y, Miyoshi S, Watanabe A, Shiraiwa K, Mitamura H, Kodama I, Ogawa S. Anisotropic conduction properties in canine atria analyzed by high-resolution optical mapping: preferential direction of conduction block changes from longitudinal to transverse with increasing age. *Circulation*. 2002;105:2092–2098.

CLINICAL PERSPECTIVE

Autonomic dysfunction has an important role in the development of atrial fibrillation (AF). Recent studies showed the importance of the intrinsic cardiac neural network, a subdivision of the autonomic nervous system in the pathogenesis of AF. The present study provides experimental evidence that vasoactive intestinal polypeptide, a neurotransmitter with 28 amino acids that is coreleased from intrinsic cardiac neurons, with the more traditionally known transmitter, acetylcholine, shortens atrial action potential durations and reduces conduction velocities with increased spatial action potential duration heterogeneities and, thereby, increases vulnerability to AF in dogs. Vasoactive intestinal polypeptide has direct actions on ionic channels, including increasing the delayed rectifier K^+ current and L-type calcium current and decreasing outward potassium currents and the sodium current. We also provide human data that support similar vasoactive intestinal polypeptide effects in human atria. Therefore, our study provides new insights to the pathophysiology of AF and may provide new therapeutic target in the clinical management of AF.

SUPPLEMENTAL MATERIAL

EXPANDED METHODS

Isolation of canine atrial cardiomyocytes

Canine atria with coronary artery perfusion were perfused with modified Tyrode's solution which contained (mmol/L) 126 NaCl, 5.4 KCl, 0.8 $MgCl_2$, 10 glucose, and 10 HEPES, (pH 7.4 adjusted with NaOH), to eliminate the blood cells and most of calcium. Then the digestion solution with 300 IU/ml collagenase type II, 0.03% protease with 0.1% bovine serum albumin was perfused for about 30 min, following by a 10 min washout period with calcium-free Tyrode's solution. The tissues from left atrial free wall were dissociated in Kraftbrühe (KB) solution at room temperature (22~24°C) with the following composition (mmol/L): 25 KCl, 10 KH_2PO_4, 3 $MgCl_2$, 10 glucose, 0.5 EGTA, 20 Taurine, 70 L-Glutamic acid, and 10 HEPES (pH 7.35 adjusted with KOH). After the extra tissues were filtered out, the rod-shaped and round myocytes were suspended and stored in KB solution in 4°C for 1 hour to stabilize them before patch clamp experiments.

Whole-cell patch clamp technique

For action potential recording, the perforated patch technique with pipette solution containing amphotericin B (240 mg/L, Sigma, MO) was used. The currents were recorded by the conventional ruptured patch-clamp method following onset step-pulse voltages which were generated with Axopatch 700A amplifier using pCLAMP 9 software (Molecular Device, CA) with Bessel low-pass filter (cut-off frequency: 10 kHz) and with a sampling frequency of 10 kHz for I_{Kur}, I_{to}, I_{Na} and $I_{Ca,L}$, and 2 kHz for I_{Kr}, I_{Ks}. All data were analyzed using Clampfit (Axon Instruments, CA) and Igor software (WaveMetrics, OR).

The pipette solution used to record action potential and K^+ current contained (mmol/L): 120 K-Asparatate, 10 Na_2ATP, 2 $MgCl_2$, 10 EGTA and 10 HEPES (pH 7.35 adjusted with KOH). For action potential recording, Tyrode's solution was perfused as bath solution.

For all potassium currents, nifedipine (2 nmol/L) was added to block the calcium currents and atropine (200 nmol/L) was used to eliminate any basal activity of acetylcholine-dependent K^+

current. A pre-pulse from holding potential -80 mV to -40 mV for 20 msec was used to inactive sodium current.

For recording of delayed rectified K^+ current, 4-AP (2 μmol/L) was added to block transient K^+ current, I_{to}, and I_{Kur}. I_{Ks} was evoked by a step-pulse protocol (between –60 mV and 60 mV for 5 second) in the presence of E-4031 (10 μmol/L), a highly selective blocker of I_{Kr}. I_{Kr} was recorded with same protocol and pipette solution as for I_{Ks} and E-4031 was replaced by chromanol 293B (30 μmol/L) in the bath solution to block I_{Ks}.

The transient outward K^+ currents were recorded with a short depolarizing pulse of 500 msec from -60 mV to 60 mV with a holding potential of -80 mV. The short depolarizing pulse and chromanol 293B (30 μmol/L) and E-4031 (10 μmol/L) were used to minimize I_{Ks} and I_{Kr}, respectively. Another protocol with a pre-pulse at 40 mV for 100 ms, which inhibits I_{to}, was used to determine ultra-rapid delayed rectifier K^+ current (I_{Kur}). Then transient outward currents (I_{to}) was then derived as the difference in current by subtracting I_{Kur} elicited by a step pulse from the holding potential of -80 mV with a 40 mV pre-pulse from the total transient outward K^+ current elicited without such pre-pulse (Figure 2).[1]

For I_{K1}, nifedipine (2 nmol/L) was added to block the calcium currents and atropine (200 nmol/L), to eliminate any basal activity of acetylcholine-dependent K^+ current. I_{K1} was measured as the 0.5 mmol/L Ba^{2+}-sensitive current upon 300-msec pulses from a holding potential of -80 mV to voltages ranging from -10 to -120 mV at 10 mV steps.

The pipette solution to record I_{Na} contained (mmol/L): 5 NaF, 115 CsF, 20 CsCl, 10 EGTA and 10 HEPES (pH 7.35 adjusted with CsOH). Bath solution contained (mmol/L): 5 NaCl, 1 $MgCl_2$, 130 tetraethylammonium chloride (TEACl), 5 CsCl, 10 HEPES, and 10 glucose (pH 7.35 adjusted with NaOH). I_{Na} was elicited by step pulse protocol (between -100 mV and 30 mV for 20 msec from a holding potential of -120 mV). For voltage-dependence of peak conductance of I_{Na}, conductance G (V) was calculated by the equation: $G(V) = I / (V_m - E_{rev})$, where I is the peak current, E_{rev} is the measured reversal potential, V_m is the membrane potential. The normalized

peak conductance was plotted against membrane potentials. Steady-state inactivation of I_{Na} was estimated by a prepulse protocol (between –140 mV and -40mV for 500 msec from a holding potential of -140 mV). The normalized peak currents tested at -40 mV were plotted as a function of prepulse potentials. Steady state activation and inactivation were fitted with the Boltzmann equation: $y = [1 + \exp((V_h - V_m)/k)]^{-1}$, where y represents variables; V_h, midpoint; k, slope factor; V_m, membrane potential.

For the $I_{Ca,\,L}$ recording, the intracellular pipette contained (mmol/L): 85 K-Asparatate, 20 TEACl, 2 $MgCl_2$, 10 EGTA, 10 HEPES, 5 Mg-ATP, and 5 Na_2-GTP (pH 7.2 adjusted with KOH). The extracellular buffer contained (mmol/L): 135 NaCl, 1 $MgCl_2$, 1.8 $CaCl_2$, 5.4 KCl, 10 HEPES, and 10 glucose (pH 7.35 with NaOH). Whole-cell $I_{Ca,\,L}$ traces were induced by a step pulse protocol (between -40 and 40 mV for 500 msec from a holding potential of -80mV after 40 ms prepulse at -40 mV). $I_{Ca,\,L}$ was calculated as the difference between peak currents and the steady-state currents at the end of test pulse. For voltage-dependence of peak conductance of $I_{Ca,\,L}$, conductance G (V) was calculated by the same equation for I_{Na}. Steady-state inactivation of $I_{Ca,\,L}$ was estimated by a prepulse protocol (between -60 and 20 mV for 2 seconds). The normalized peak currents were plotted as a function of prepulse potentials. The normalized peak currents were plotted as a function of prepulse potentials. Steady state activation and inactivation were fitted with the Boltzmann equation.

Optical mapping

The voltage-sensitive dye, RH237 (Molecular Probes, OR), was dissolved in dimethylsulfoxide (DMSO, 2 mmol/L, Sigma, MO) to stain atrial tissue immediately prior to recording. Electromechanical uncoupling agent blebbistatin (20 μmol/L, Cayman, MI) was employed to eliminate motion artifact. Two custom-made light-emitting diode modules were used as light source for photoexcitation. The optical signals were collected from intensified images recorded through charge-coupled device cameras (model TM-6724, Pulnix Inc., CA) with a 700 nm long-

pass filter (Newport Co., CA) at 711 frames/sec, acquired from 120×160 sites over a 15×20 mm^2 area in the left atrial free wall (Figure 2A).

The optical image dataset was processed with custom-designed software based on Matlab platform and features such as activation sequence map and action potential duration (APD) map were extracted as previously described.[2] Local activation time was identified as the point at which the maximum first derivative (dF/dt_{max}) occurred during the optical action potential upstroke. Isochronal maps of activation were generated from activation time data. To determine APD, the peak signal following the upstroke was identified. Steady state APD was defined as the interval between the local activation time and the time when the optical signal had recovered or "repolarized" by a given percentage from their peak value, i.e., 20% (APD_{20}), 50% (APD_{50}), 75% (APD_{75}), and 90% (APD_{90}) of full repolarization. For each map, the average APD and the standard deviation of the APDs within the mapped area were calculated. The standard deviation of the APDs values in each map was used as a measure of the spatial dispersion of APD. Phase maps were constructed with a time-delay embedding method.[3]

Local conduction velocity

To measure local conduction velocity (CV), we employed the algorithm described by Bayly et al.[4] Briefly, the distribution of local activation times in a 5x5 pixel region were fitted to a polynomial plane where the gradients, gx and gy, of activation time for the region were calculated along the x and y axes, respectively. The magnitude of the local CV for each pixel was defined as $(gx^2+gy^2)^{1/2}$. Standard deviation of CV (CV-SD) was used as a measurement of spatial heterogeneity of conduction velocity.

Inducibility of AF

Atrial vulnerability to AF was assessed by the inducibility of AF with programmed stimulation (up to 3 extra stimuli) after a 20 beat pacing train at a basic drive cycle length (DCL) of 200 msec. The initial coupling interval for each extra stimulus was set >50 msec longer than the atrial effective refractory period (AERP) with 1-msec decrements in subsequent stimulations. AERP

was defined as the longest coupling interval that failed to capture the atrial myocardium. AF was considered induced if there were disorganized atrial electrical activities with varying cycle lengths and changing electrographic morphologies lasting more than 2 sec.[5]

SUPPLEMENTAL EXPERIMENTS

Methods

Isolation of human atrial cardiomyocytes for patch clamping

Human atrial tissue (left appendage) samples were obtained during mitral valve replacement surgery for individuals with normal left ventricular function and without rheumatic heart disease. Informed consent was obtained prior to the surgery, as approval by the Institutional Review Board at the Texas Heart Institute. Only patients without diagnosis of atrial fibrillation were select for this study. Human atrial myocytes were isolated enzymatically from left atrial tissues of the above-described patients using a modified technique, as described previously.[6] Briefly, atrial tissue was chopped into cubic chunks (about 2 mm^3) in Ca^{2+}-free Tyrode's solution (4 °C), and then washed in a 50 ml tube containing 10 ml of the Ca^{2+}-free Tyrode's solution (36 °C), and continuously bubbled with 100% O_2 for 20 min (exchanging solution every 5 min). The chunks were digested in a Ca^{2+}-free Tyrode's solution containing 150 U/ml collagenase (Type II, Worthington Biochemical, NJ), 2 U/ml protease (Type XXIV, Sigma, MO) and 0.1% bovine serum albumin (Sigma, MO) for 50 min. Then the chunks were switched to a fresh enzyme solution as described above, but without protease. The medium was examined microscopically at 5 to 10 min interval to determine the number and quality of the isolated cells. When the yield appeared to be maximal, the chunks were suspended in a KB storage solution (as above) and gently pipetted. The isolated myocytes were kept at 4 °C in KB storage solution for about 60 min before patch-clamp experiments were performed.

Immunofluorescence staining of canine atrial cardiomyocytes

We harvested atrial cardiomyocytes from the left atrial appendage where the optical mapping study was performed. Isolated canine atrial cardiomyocytes attached to gelatin-coated slides were fixed with paraformaldehyde (4%) at room temperature for 30 minutes, blocked with CAS-blocker (Invitrogen, CA), then stained with primary antibodies (anti-$VPAC_1$ or -$VPAC_2$, Abcam, MA and anti-α-actinin, Sigma, MO) at a 1:400 dilution for 1 hour and then incubated with the corresponding Alexa Flour 488- or 594-conjugated secondary antibody (Molecular Probes, CA) for 30 minutes. Sections were mounted with prolonged gold antifade reagent (Molecular Probes, CA) and visualized using a Leica HCS laser scanning confocal microscope (Leica, Wetzlar, Germany) with z-stack scanning of the entire cell membrane.

Results

VIP shortens action potential duration of human atrial myocytes

To validate the relevance of VIP's effects on canine atrial APD to human conditions, we investigated the effects of VIP on action potentials of human atrial cardiomyocytes isolated from the left atria during open-heart surgery. Action potentials were elicited at two frequencies, 0.1 Hz and 1 Hz, at room temperature using the perforated current-mode patch clamp technique. Only healthy cells (n=18 from 10 patients) with a stable resting potential of less than -70 mV were chosen for the study. As shown in **Figure S1**, VIP (1 μmol/L) significantly shortened the APD in comparison with the baseline (APD_{75} at 0.1 Hz: 139 ± 24 msec, *vs.* 156 ± 22 msec at baseline, $p < 0.01$; at 1 Hz: 121 ± 13 msec *vs.* 145 ± 15 msec at baseline, $p<0.01$, n=18), an effect that was reversed after washout. The APD_{75} after 15-minute washout was 158 ± 24 at 0.1 Hz msec and 141 ± 15 msec at 1 Hz, which was significantly longer in comparison with APD during VIP perfusion, $p<0.01$, but not significantly different from the baseline, $p = 0.82$ and 0.22, respectively. VIP did not significantly affect the resting potential (-79.69 ± 2.42 mV with 1 μmol/L VIP *vs.* -80.67 ± 2.34 mV at baseline $p = 0.40$) or the amplitudes (133.75 ± 20.19 mV with 1 μmol/L VIP *vs.* 137.32 ± 20.16 mV at baseline, $p = 0.81$).

Heterogeneous expression of VIP receptors in canine atrial cardiomyocytes

Immunofluorescence staining was performed on canine atrial myocytes isolated to assess VIP receptor expression (Figure S2). Fine structural elements of cardiac sarcomeric α-actinin were visualized by staining with anti-α-actinin antibody: an even distribution of sarcomeres was observed in all cardiomyocytes. However, the VIP receptors, $VPAC_1$ and $VPAC_2$, were not uniformly present in all cardiomyocytes (Figures S2B and S2E). The percentage of VPAC positive atrial myocytes were evaluated by counting 5 random microscope fields per slides from 7 dogs (two slide per dog, one for VPAC1 and one for VPAC2, respectively), comparing to the total α-actinin positive cells. Anti-VPAC1 antibody detected in 62.2% myocytes (82.5 ± 37.0 VPAC1 positive cells out of 132.6 ± 65.9 total α-actinin positive cells per slide), and anti-VPAC2 antibody detected in 78.6% positive myocytes (90.5 ± 35.6 VPAC2 positive cells out of 115.1 ± 40.3 total α-actinin positive cells per slide).

References

1. Brouillette J, Clark RB, Giles WR, Fiset C. Functional properties of k+ currents in adult mouse ventricular myocytes. *J Physiol*. 2004;559:777-798
2. Yuan X, Uyanik I, Situ N, Xi Y, Cheng J. Coi-wiz: An interactive computer wizard for analyzing cardiac optical signals. *Conf Proc IEEE Eng Med Biol Soc*. 2009;2009:1828-1831
3. Bray MA, Lin SF, Aliev RR, Roth BJ, Wikswo JP, Jr. Experimental and theoretical analysis of phase singularity dynamics in cardiac tissue. *J Cardiovasc Electrophysiol*. 2001;12:716-722
4. Bayly PV, KenKnight BH, Rogers JM, Hillsley RE, Ideker RE, Smith WM. Estimation of conduction velocity vector fields from epicardial mapping data. *IEEE Trans Biomed Eng*. 1998;45:563-571
5. Wyndham CR, Amat-y-Leon F, Wu D, Denes P, Dhingra R, Simpson R, Rosen KM. Effects of cycle length on atrial vulnerability. *Circulation*. 1977;55:260-267
6. Li GR, Feng J, Wang Z, Nattel S. Transmembrane chloride currents in human atrial myocytes. *American Journal of Physiology - Cell Physiology*. 1996;270:C500-C507

Supplemental Figure Legends

Figure S1. Effect of VIP on APDs of human atrial cardiomyocytes. A. Representative recordings of action potentials from human atrial myocytes at 1 Hz. **B.** The reversible shortening and the typical time course of APD_{75} at 1 Hz in response to VIP are shown. Open circles indicate the representative traces in panel A. **C.** The composite data shows that VIP (1 µmol/L) shortens APD_{75} both at 0.1 and 1 Hz. **p<0.01 *vs.* baseline; $^{\#\#}$p<0.01 *vs.* wash-out.

Figure S2. Expression of VIP receptors on atrial cardiomyocytes. Immunofluorescence of α-Actinin (**A, D**), $VPAC_1$ (**B**), $VPAC_2$ (**E**), and merged images (**C, F**) of canine atrial myocytes showing variable expression of VIP receptors ($VPAC_1$ and $VPAC_2$): α-Actinin was visualized using anti-mouse Alexa Flour 594 (red**, A and D**) and the VIP receptors, anti-rabbit Alexa Flour 488 (green**, B and E**). Areas of overlapping expression of Actinin and the respective VIP receptor is shown in yellow (**C and F**). $VPAC_1$, $VPAC_2$, vasoactive intestinal polypeptide receptor 1 and 2.

Figure S1

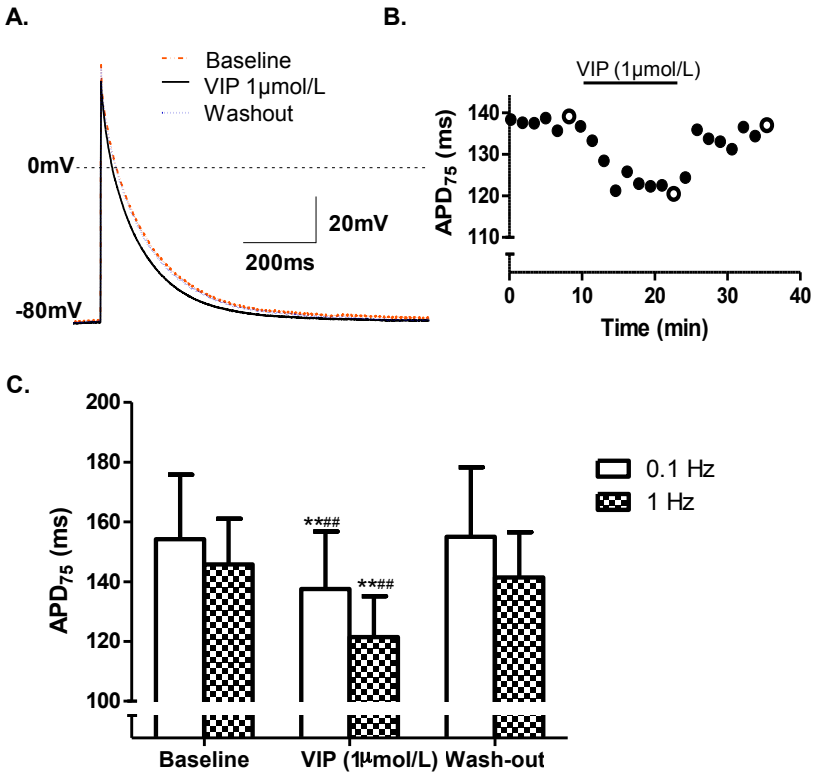
A.
B.
Baseline
VIP 1μmol/L
Washout
0mV
-80mV
20mV
200ms
VIP (1μmol/L)
APD75 (ms)
140
130
120
110
0
10
20
30
40
Time (min)
C.
200
180
160
140
120
100
APD75 (ms)
**##
**##
0.1 Hz
1 Hz
Baseline
VIP (1μmol/L)
Wash-out

Figure S2

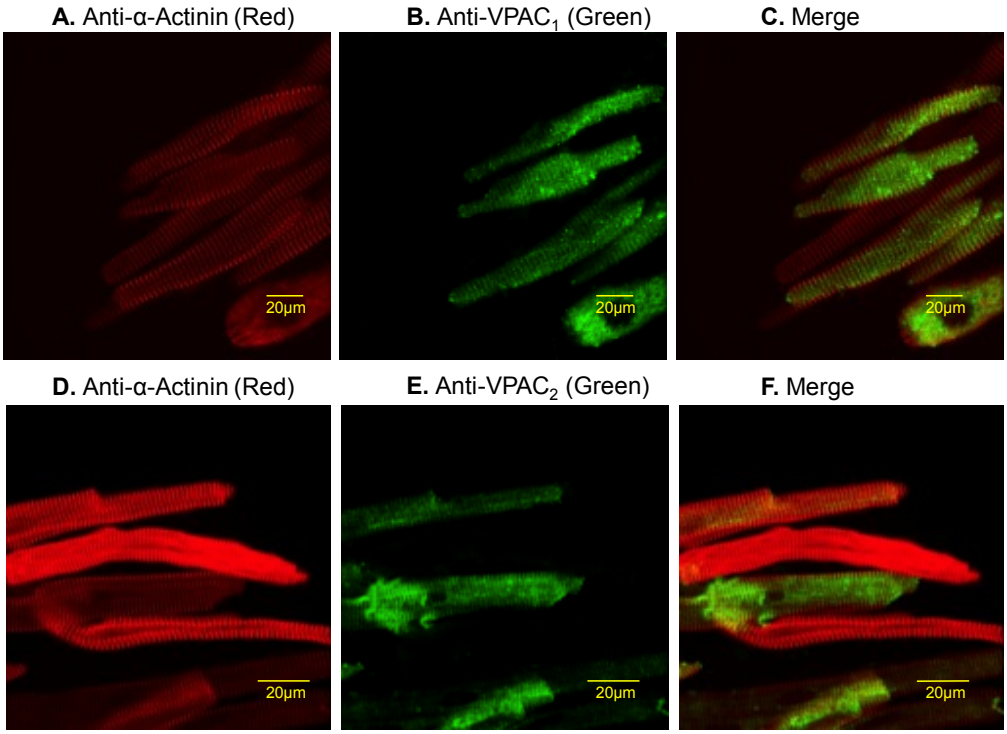
A. Anti-α-Actinin (Red)
B. Anti-VPAC1 (Green)
C. Merge
D. Anti-α-Actinin (Red)
E. Anti-VPAC2 (Green)
F. Merge
20μm

SUPPLEMENTAL DATA

Table S1. Parameters of K^+ channels

	Baseline	VIP (1 μmol/L)	Washout
I_{Ks} (n=13 cells)			
Peak current density at 60 mV (pA/pF)	6.88 ± 0.97	12.78 ± 1.48$^{**\#\#}$	6.90 ± 0.95
Tail current density at 20 mV (pA/pF)	0.49 ± 0.03	0.68 ± 0.03$^{*\#}$	0.53 ± 0.04
I_{Kr} (n=7 cells)			
Peak current density at 20 mV (pA/pF)	1.33 ± 0.05	1.28 ± 0.06	1.29 ± 0.06
Tail current density at 20 mV (pA/pF)	1.02 ± 0.06	0.98 ± 0.05	1.03 ± 0.05
I_{Kur} (n=11 cells)			
Peak current density at 60 mV (pA/pF)	5.95 ± 0.68	3.29 ± 0.26$^{*\#}$	5.50 ± 0.99
I_{to} (n=11 cells)			
Peak current density (pA/pF)	3.65 ± 0.48	1.13 ± 0.14$^{**\#\#}$	2.68 ± 0.43

All data are presented as mean ± standard error of mean (S.E.M.) *p<0.05, **p<0.01 *vs.* baseline, $^{\#}$p<0.05, $^{\#\#}$p<0.01 *vs.* washout.

Table S2. The effect of VIP on kinetics of sodium current (I_{Na}) and L-type calcium current ($I_{Ca,\,L}$).

	Baseline	VIP (1 μmol/L)	Washout
I_{Na} (n=16 cells)			
Peak current density (pA/pF)	-34.60 ± 1.5	-26.92 ± 1.4**#	-32.14 ± 1.8
Activation V_h (mV)	-50.05 ± 0.2	-45.17 ± 0.3**#	-49.91 ± 0.3
Activation *k*	6.05 ± 0.2	5.89 ± 0.3	4.84 ± 0.3
Fast-inactivation V_h (mV)	-95.97 ± 0.8	-100.09 ± 1.1**##	-94.86 ± 0.8
Fast-inactivation *k*	7.38 ± 0.7	9.21 ± 0.9	8.48 ± 0.7
$I_{Ca,\,L}$ (n=11 cells)			
Peak current density (pA/pF)	-10.54 ± 1.3	-14.11 ± 1.7**##	-10.08 ± 1.2
Activation V_h (mV)	-5.28 ± 0.6	-7.79 ± 0.6*#	-6.95 ± 0.5
Activation *k*	6.24 ± 0.5	4.99 ± 0.6	6.38 ± 1.0
Fast-inactivation V_h (mV)	-21.65 ± 1.1	-25.45 ± 0.8*#	-22.00 ± 0.8
Fast-inactivation *k*	7.60 ± 0.9	5.53 ± 0.7	5.71 ± 0.7

All data are presented as mean ± S.E.M. *p<0.05, **p<0.01 vs. baseline, #p<0.05, ##p<0.01 vs. washout.

Table S3. Mean action potential duration of canine atria at multiple VIP concentrations

APD (ms)	DCL (ms)	Baseline	VIP 0.1μmol/L	VIP 1μmol/L	VIP 10μmol/L	Washout	*p* value
APD_{20}	200 ms	45 ± 4	41 ± 4	39 ± 3	39 ± 3*	43 ± 3	<0.01
	300 ms	50 ± 4	44 ± 4	40 ± 4	41 ± 5	44 ± 3	
	400 ms	51 ± 4	39 ± 4	42 ± 5	38 ± 5	40 ± 2	
	500 ms	47 ± 5	39 ± 5	45 ± 3	59 ± 5	42 ± 5	
APD_{50}	200 ms	75 ± 7	83 ± 8	65 ± 7	67 ± 7	83 ± 6	<0.01
	300 ms	88 ± 6	90 ± 8	73 ± 7	75 ± 8	88 ± 9	
	400 ms	78 ± 5	86 ±5	78 ± 11	71 ± 11	81 ± 11	
	500 ms	83 ± 3	79 ± 6	68 ± 8	74 ± 8	95 ± 11	
APD_{75}	200 ms	113 ± 4	105 ± 9	77 ± 7$^{**\#\#}$	88 ± 12$^{**\#\#}$	124 ± 13	<0.001
	300 ms	131 ± 9	117 ± 8*	102 ± 10*	92 ± 7**	107 ± 8	
	400 ms	132 ± 9	112 ± 7*	109 ± 9	102 ± 12*	117 ± 8	
	500 ms	142 ± 9	111 ± 11**	89 ± 11$^{**\#\#}$	98 ± 9$^{**\#}$	118 ± 5	
APD_{90}	200 ms	126 ± 6	115 ± 7	88 ± 8$^{*\#}$	103 ± 12$^{*\#b}$	129 ± 16	<0.001
	300 ms	141 ± 9	138 ± 10	117 ± 9$^{*\#b}$	115 ± 12$^{*\#b}$	138 ± 12	
	400 ms	156 ± 13	131 ± 7$^{*\#b}$	125 ± 8$^{*\#b}$	111 ± 12$^{*\#a}$	142 ± 11	
	500 ms	172 ± 11	138 ± 14$^{*\#a}$	108 ± 9$^{*\#b}$	119 ± 3$^{*\#a}$	151 ± 10	

Note:

1) The APD_{20}, APD_{50}, APD_{75}, APD_{90} represent action potential duration (APD) at 20%, 50%, 75%, and 90% of full repolarization. VIP; All data are presented as mean ±standard error of the mean (S.E.M.). The data was collected from 8 canine atria.
2) VIP: Vasoactive intestinal polypeptide; DCL, Drive cycle length.
3) p value: p values derived from a mixed effect model which was developed with proc mixed procedure with individual cells as random factor and different VIP concentrations, DLCs levels as fixed effects..
4) Each APD data point during VIP perfusion was compared by the from a mixed effect model with the baseline ($^{*}p<0.05$) or with washout ($^{\#}p<0.05$). Our data may indicate (1) VIP affects late repolarization more than the early repolarization, likely in part due to its competing effects of reducing I_{to} and increasing I_{Ks} during early repolarization (2) there is a dose-dependent VIP effect that was only partially recovered after washout, suggesting

a complex post-synaptic process with residual effects lingering after VIP is dissociated from its receptor.

Table S4. Mean action potential duration of canine atria in 1 hour time span

APD (ms)	DCL (ms)	0 min	15 min	30 min	45 min	60 min
APD_{20}	200	40 ± 0	39 ± 2	45 ± 3	38 ± 3	43 ± 5
	300	38 ± 7	43 ± 3	41 ± 4	35 ± 4	39 ± 4
	400	45 ± 8	43 ± 3	40 ± 6	36 ± 4	41 ± 6
	500	41 ± 3	37 ± 5	36 ± 3	37 ± 10	47 ± 10
APD_{50}	200	83 ± 5	73 ± 7	88 ± 2	74 ± 6	79 ± 10
	300	88 ± 11	86 ± 6	84 ± 5	72 ± 15	87 ± 15
	400	91 ± 10	96 ± 9	87 ± 4	96 ± 14	96 ± 17
	500	97 ± 12	95 ± 9	88 ± 6	93 ± 16	97 ± 18
APD_{75}	200	104 ± 6	93 ± 8	105 ± 7	97 ± 7	105 ± 14
	300	113 ± 14	114 ± 7	123 ± 6	129 ± 16	116 ± 19
	400	129 ± 13	131 ± 14	129 ± 9	129 ± 17	120 ± 22
	500	132 ± 14	128 ± 13	123 ± 10	132 ± 20	129 ± 24
APD_{90}	200	122 ± 4	117 ± 5	123 ± 11	116 ± 6	123 ± 15
	300	134 ± 16	139 ± 9	152 ± 7	137 ± 26	144 ± 19
	400	151 ± 12	165 ± 18	138 ± 13	165 ± 17	157 ± 23
	500	169 ± 17	169 ± 17	157 ± 11	163 ± 23	172 ± 26

All data are presented as mean ± S.E.M., n=4 dogs. Abbreviations are identical to those in Table S3.

Ionic Mechanisms Underlying the Effects of Vasoactive Intestinal Polypeptide on Canine Atrial Myocardium

Yutao Xi, Geru Wu, Tomohiko Ai, Nancy Cheng, Jurij Matija Kalisnik, Junping Sun, Shahrzad Abbasi, Donghui Yang, Christopher Fan, Xiaojing Yuan, Suwei Wang, MacArthur Elayda, Igor D. Gregoric, Bharat K. Kantharia, Shien-Fong Lin and Jie Cheng

Circ Arrhythm Electrophysiol. 2013;6:976-983; originally published online September 17, 2013;
doi: 10.1161/CIRCEP.113.000518
Circulation: Arrhythmia and Electrophysiology is published by the American Heart Association, 7272 Greenville Avenue, Dallas, TX 75231

Print ISSN: 1941-3149. Online ISSN: 1941-3084